Volume 8 | Number 46 | 14 December 2017 | Pages 7079–7280

Polymer Chemistry

rsc.li/polymers

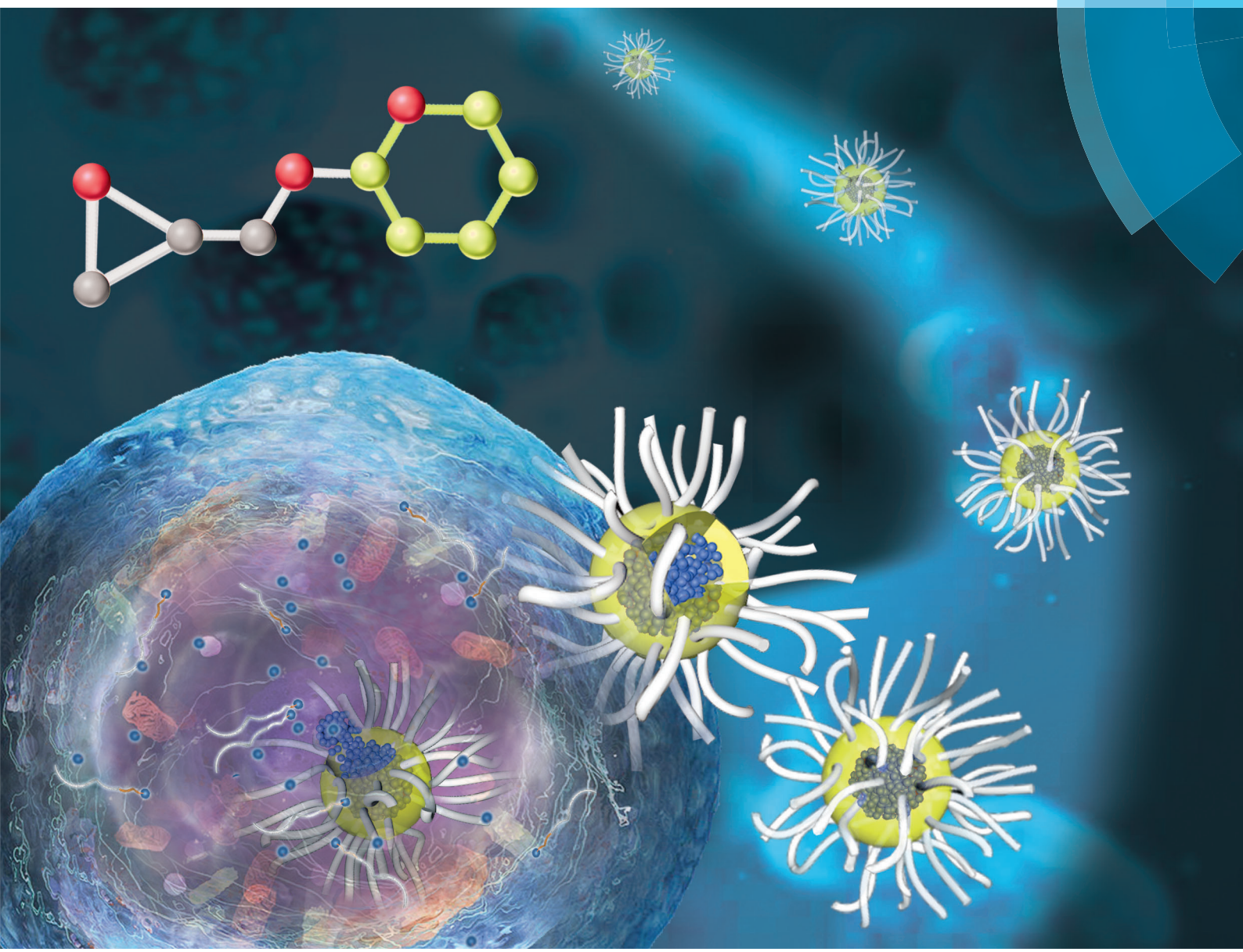

ISSN 1759-9962

ROYAL SOCIETY OF CHEMISTRY

PAPER

Byeong-Su Kim *et al.*

The power of the ring: a pH-responsive hydrophobic epoxide monomer for superior micelle stability

Polymer Chemistry

PAPER

View Article Online
View Journal | View Issue

Cite this: *Polym. Chem.*, 2017, **8**, 7119

The power of the ring: a pH-responsive hydrophobic epoxide monomer for superior micelle stability†

Jaeeun Song,[a] L. Palanikumar,[a] Yeongkyu Choi,[a] Inhye Kim,[b] Tae-young Heo,[c] Eungjin Ahn,[d] Soo-Hyung Choi,[c] Eunji Lee,[b] Yuji Shibasaki,[e] Ja-Hyoung Ryu[a] and Byeong-Su Kim*[a,d]

Received 20th September 2017,
Accepted 5th October 2017

DOI: 10.1039/c7py01613a

rsc.li/polymers

Despite the growing interest in amphiphilic block copolymers for their application in micelles as ideal drug delivery carriers, there remain some challenges related to biocompatibility, stability, degradability, and loading efficiency of the micelles. Herein, we report a novel hydrophobic, pH-responsive epoxide monomer, tetrahydropyranyl glycidyl ether (TGE). Anionic ring-opening polymerization affords the controlled synthesis of a series of its homopolymers (PTGE) and amphiphilic polymers, poly(ethylene glycol)-*block*-poly(tetrahydropyranyl glycidyl ether) (PEG-*b*-PTGE). Interestingly, these block copolymers with cyclic TGE moieties showed superior stability in biological media, high loading capacity, tunable release, and controllable degradation compared to the block copolymers with its acyclic analogue, 1-ethoxyethyl glycidyl ether (EEGE), widely employed in polyether, which satisfy all the required design principles and address the challenges in drug delivery systems. The superior biocompatibility coupled with the high stability of the novel functional epoxide monomer is anticipated to lead to the development of a versatile platform for smart drug delivery systems.

1. Introduction

The self-assembly of amphiphilic molecules has generated considerable interest due to their potentially wide-ranging applications in detergents, templates, and catalysts, to drug delivery.[1–3] Polymeric amphiphiles like amphiphilic block copolymers have garnered particular attention due to their high physical and chemical tunability in each block from the respective monomer, which in turn allows one to tailor the stability and functionality of the resulting self-assembled nanostructures. Among these, polymeric micelles self-assembled in aqueous solutions have been exploited as ideal drug delivery carriers, some of which, such as Pluronics, Paclical, and Genexol-PM, have advanced successfully to clinical settings.[4,5]

Besides the important stabilizing role of the hydrophilic block, the self-assembly of polymeric micelles is governed by the choice of the hydrophobic block. In particular, the properties of the hydrophobic blocks determine the stability, degradability, and loading efficiency of the resulting micelles. For example, polymeric micelles often undergo dynamic dissolution at high dilution and exposure to changes in pH and salt concentration upon systemic injection to the blood stream.[6] Accordingly, there have been active investigations for tailoring many synthetic parameters affecting the stability of micelles, including crystallinity,[7,8] stereoregularity,[9] molecular weight, and substituents[10–13] on the hydrophobic block. Sophisticated delivery is another critical factor to consider. Together with the development of micelles responsive to external stimuli like pH, light, redox, and temperature,[14–20] control over the release profile of the internal payload has been explored by introducing new structures in the hydrophobic block.[21–25] Thus, it can be concluded that the hydrophobic block in amphiphilic block copolymers plays a key role in modulating the critical parameters of polymeric micelles.

[a]*Department of Chemistry, Ulsan National Institute of Science and Technology (UNIST), Ulsan 44919, Korea. E-mail: bskim19@unist.ac.kr*
[b]*Graduate School of Analytical Science and Technology, Chungnam National University, Daejeon 34134, Korea*
[c]*Department of Chemical Engineering, Hongik University, Seoul 04066, Korea*
[d]*Department of Energy Engineering, Ulsan National Institute of Science and Technology (UNIST), Ulsan 44919, Korea*
[e]*Department of Chemistry and Bioengineering, Faculty of Engineering, Iwate University, 4-3-5 Ueda, Morioka, Iwate 020-8551, Japan*

†Electronic supplementary information (ESI) available: Detailed ^{1}H, ^{13}C, COSY, and HSQC NMR spectra of the monomer, and the GPC trace and DSC graphs of the synthesized polymers. Excitation spectra of pyrene for CMC measurement. DLS, SAXS, AFM, TEM, and cryo-TEM of the micelles. Emission spectra of DiO and DiI for the FRET test and *in vitro* FRET studies. Excitation spectra of pyrene under acidic conditions. Paclitaxel encapsulation efficiency and *in vitro* cell viability. See DOI: 10.1039/c7py01613a

Therefore, it continues to be a challenging endeavor to develop a novel hydrophobic block monomer to achieve the aforementioned high tunability of the micelles for drug delivery systems.

For biomedical applications of micelles, poly(ethylene glycol) (PEG) is by far the most frequently employed as a hydrophilic block to provide aqueous stability owing to its superior solubility, biocompatibility, low immunogenicity, and stealth effect.[26,27] As an alternative to PEG, its polyether analogue, polyglycerol (PG), has attracted attention due to its biocompatibility and other advantages over PEG, such as a controllable structure, functional group, and facile synthesis.[28–34] To date, diverse epoxide monomers have been developed with tunable physicochemical properties and functionalities.[17,19,35–39]

Herein, we report the design and synthesis of a novel epoxide monomer, tetrahydropyranyl glycidyl ether (TGE), and a series of its homopolymers (PTGE) and amphiphilic polymers, poly(ethylene glycol)-*block*-poly(tetrahydropyranyl glycidyl ether) (PEG-*b*-PTGE), employing the TGE block as a pH-responsive hydrophobic block (Fig. 1 and Table 1). The molecular design of TGE satisfies all the required design principles and addresses the challenges encountered in drug delivery systems to achieve highly tunable polymeric micelles with high stability, loading capacity, tailorable release, and degradability. Moreover, this novel epoxide monomer system can produce well-defined polymers with all-polyether backbones possessing superior flexibility and biocompatibility unlike other all-

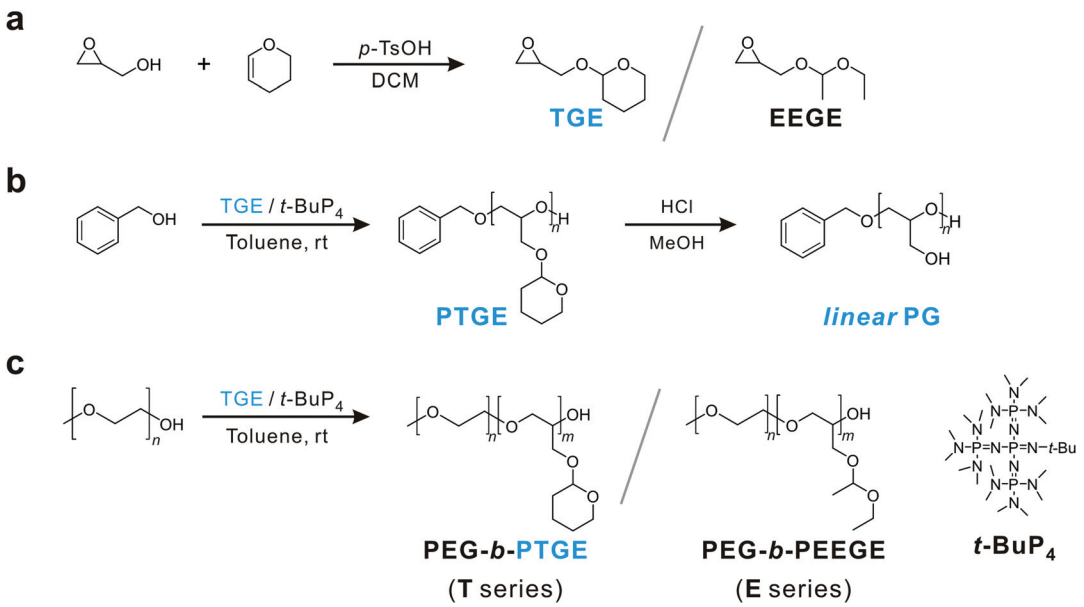

Fig. 1 Synthetic scheme for the (a) TGE monomer, (b) PTGE homopolymer and linear PG, and (c) PEG-*b*-PTGE block copolymer. Structures of the EEGE monomer and the PEG-*b*-PEEGE block copolymer are presented for comparison. *t*-BuP_4 was employed as a metal-free organic base for polymerization.

Table 1 Characterization data for all polymers synthesized

No		Polymer composition[a]	M_n [a] (g mol^{-1})	M_n [b] (g mol^{-1})	M_w/M_n [b]	T_g [c] (°C)	CMC[d] (mg L^{-1})
1		$PTGE_{14}$	2400	1800	1.12	−31.0	—
2		$PTGE_{20}$	3300	1900	1.03	−24.0	—
3		$PTGE_{38}$	6100	3000	1.10	−21.7	—
4		$PTGE_{118}$	18 600	6200	1.19	−20.3	—
5	**T1**	PEG_{114}-*b*-$PTGE_{18}$	8700	9800	1.05	−21.2	18.1
6	**T2**	PEG_{114}-*b*-$PTGE_{37}$	11 800	11 600	1.05	−17.0	9.79
7	**T3**	PEG_{114}-*b*-$PTGE_{72}$	18 000	19 600	1.23	−15.8	0.83
8	**E1**	PEG_{114}-*b*-$PEEGE_9$	7200	9300	1.09	−59.0	n.d.[e]
9	**E2**	PEG_{114}-*b*-$PEEGE_{22}$	9100	11 400	1.08	−59.1	96.0
10	**E3**	PEG_{114}-*b*-$PEEGE_{60}$	14 700	14 700	1.11	−59.0	10.3

[a] Determined *via* ^{1}H NMR spectroscopy. [b] Measured using GPC measurement (THF, RI signal, PS standard). [c] T_g was determined by differential scanning calorimetry (DSC) at a rate of 10 °C min^{-1}. [d] Critical micelle concentration (CMC) was calculated from fluorescence spectroscopy using pyrene as a probe. [e] Not determined.

carbon backbone systems. In contrast to its acyclic analogue, 1-ethoxyethyl glycidyl ether (EEGE), reported in the literature,[40–45] the TGE monomer with a cyclic pendant group provides superior stability, high loading capacity, and controllable degradation in polymeric micelles. The superior biocompatibility coupled with the high biological stability of our system is expected to lead to the development of a versatile platform for smart drug delivery systems.

2. Results and discussion

2.1 Monomer synthesis and polymerization of TGE

A novel hydrophobic, pH-responsive monomer TGE was synthesized in a facile, one-step procedure, starting from glycidol and 3,4-dihydropyran (Fig. 1a), and purified by fractional distillation in a typical isolated yield of 60%. The chemical structure was successfully confirmed using various NMR spectroscopic techniques, including ^{1}H, ^{13}C, correlation spectroscopy (COSY), and heteronuclear single-quantum correlation (HSQC), as well as using mass spectrometry (Fig. 2a and Fig. S1–S3 in the ESI†).

After confirming the successful synthesis of the TGE monomer, the polymerization proceeded *via* *t*-BuP$_4$ catalyzed anionic ring-opening polymerization (AROP) using benzyl alcohol as an initiator at room temperature for 1 day (Fig. 1b). The highly basic organic superbase *t*-BuP$_4$ was chosen as it allowed controlled polymerization of the PTGE homopolymers at room temperature,[46,47] while other metal-based CsOH and *t*-BuOK bases did not work for our monomer system.

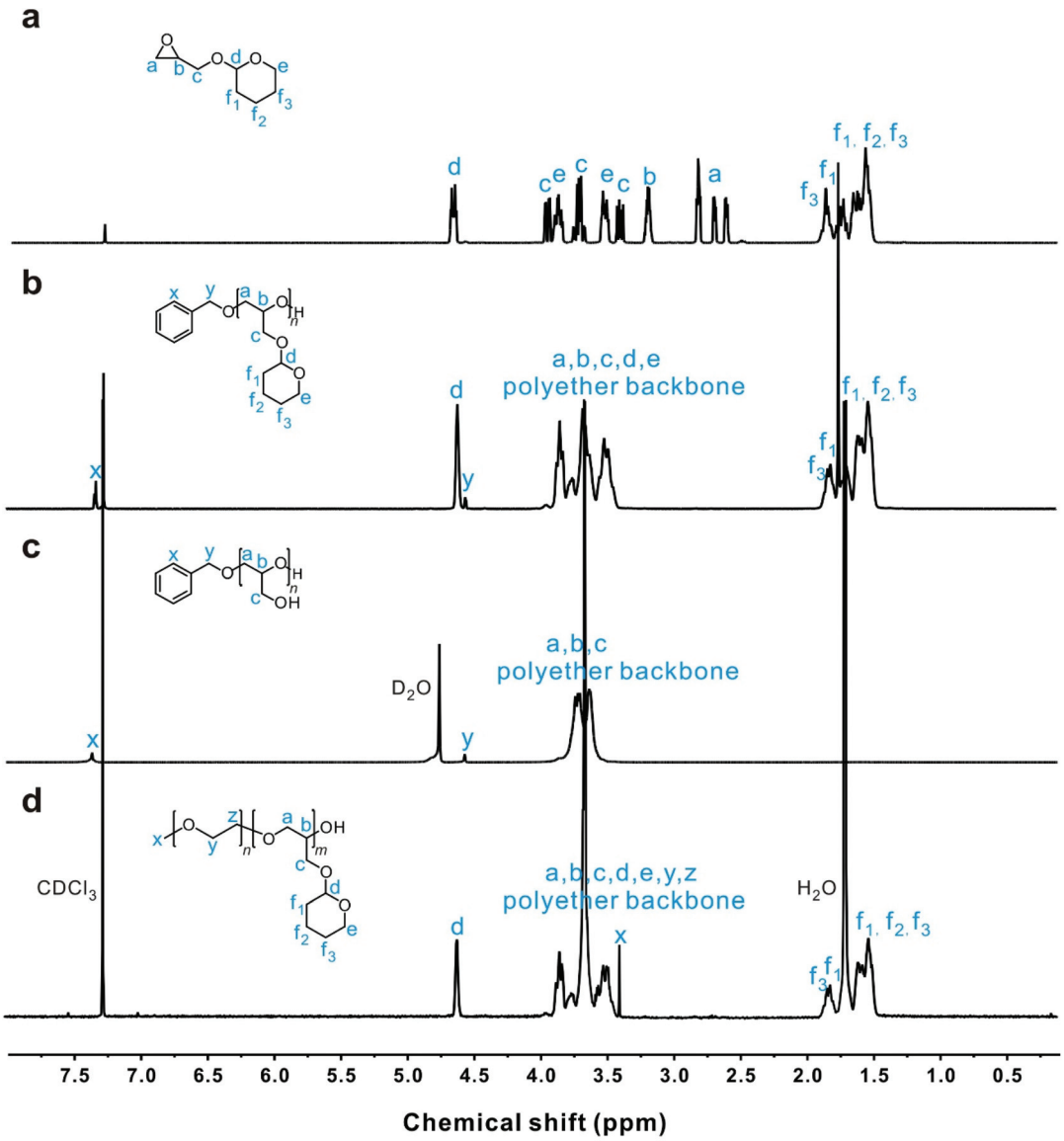

Fig. 2 Representative ^{1}H NMR spectra of the (a) TGE monomer, (b) PTGE homopolymer (entry 3 in Table 1), (c) PTGE homopolymer after deprotection, and (d) PEG-*b*-PTGE block copolymer (entry 5 in Table 1). All spectra were collected in $CDCl_3$ except (c), which was recorded in D_2O.

Here, we synthesized both the homopolymer, poly(tetrahydropyranyl glycidyl ether) (PTGE), and block copolymer, poly(ethylene glycol)-*block*-poly(tetrahydropyranyl glycidyl ether) (PEG-*b*-PTGE), using poly(ethylene glycol)monomethyl ether, mPEG ($M_{n,NMR}$ = 5900 g mol^{-1}), as the macroinitiator (Fig. 1c).

A series of PTGE homopolymers with different molecular weights ($M_{n,NMR}$ = 2400–18 600 g mol^{-1}) were successfully prepared by controlling the monomer-to-initiator ratios and were characterized by ^{1}H NMR, gel permeation chromatography (GPC), and matrix-assisted laser desorption/ionization time-of-flight (MALDI-TOF) mass spectrometry (Table 1, Fig. 2, 3 and S4†). As shown in Fig. 2b, the ^{1}H NMR spectra of PTGE clearly indicated the characteristic peaks corresponding to the aromatic initiator protons (7.30–7.38 ppm), methylene protons (4.50–4.54 ppm), polyether backbones (3.24–4.05 ppm) and tetrahydropyranyl protons (4.55–4.62 ppm and 1.44–1.91 ppm). Specifically, the number-average molecular weight ($M_{n,NMR}$) was calculated by determining the ratio of the peak integrals for the methylene group of the initiator to the tetrahydropyranyl protons (4.55–4.62 ppm) in ^{1}H NMR. After confirming the successful synthesis of PTGE polymers, they were further treated with HCl for 2 h to yield linear polyglycerol (PG) (Fig. 1b). The elimination of the tetrahydropyranyl moiety was clearly observed in the ^{1}H NMR spectrum with the disappearance of the peaks corresponding to the tetrahydropyranyl group at 1.44–1.91 ppm (Fig. 2c).

Furthermore, the GPC results of the PTGE homopolymers showed a monomodal distribution and narrow polydispersity index (M_w/M_n = 1.03–1.19), using polystyrene as a standard in THF (Table 1 and Fig. S4†). It is worth noting that the $M_{n,GPC}$ values tend to be slightly lower than the $M_{n,NMR}$ values, as shown in Table 1. This could be attributed to the hydrophobic tetrahydropyranyl side chain of the homopolymer collapsing in THF due to its higher polarity than the homopolymer, which in turn led to the difference in their hydrodynamic volumes.[48]

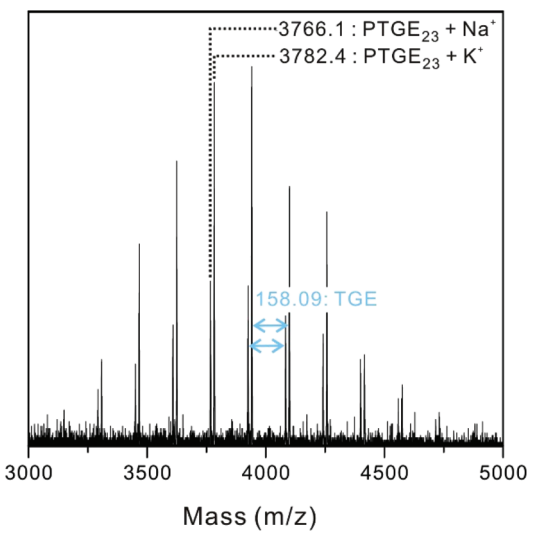

Fig. 3 Expanded MALDI-TOF mass spectrum of the $PTGE_{38}$ homopolymer (entry 3 in Table 1) from 3000 Da to 5000 Da. The spacing of the signals corresponds to the mass of the TGE monomer (158.09 g mol^{-1}) in the homopolymer. Full range of the spectrum is displayed in Fig. S5.†

To formulate the micelle and evaluate its performance as a drug delivery carrier, PEG was used as the hydrophilic block and PTGE with various molecular weights as the hydrophobic block to provide the amphiphilic block copolymers of PEG-*b*-PTGE (**T** series, Fig. 1c). The ^{1}H NMR spectrum of the amphiphilic block copolymer clearly showed the characteristic peaks of the respective blocks, including the methyl protons of mPEG (3.88 ppm), the polyether backbones (3.41–3.97 ppm), and the tetrahydropyranyl protons (4.55–4.62 ppm and 1.44–1.91 ppm) (Fig. 2d). The block copolymers of different molecular weights (8700–18 000 g mol^{-1}) were successfully prepared based on the peak integral ratio between the methyl protons of mPEG and the tetrahydropyranyl protons. The GPC results of the block copolymers also showed monomodal distributions with narrow polydispersity indexes of 1.05–1.23 (Fig. S4†). Moreover, the GPC traces of the block copolymers clearly shifted to a higher-molecular-weight region compared to the mPEG macroinitiator, revealing successful copolymerization.

As an acyclic analogue of PTGE, the amphiphilic block copolymers of poly(ethylene glycol)-*block*-poly(ethoxyethyl glycidyl ether) (PEG-*b*-PEEGE) were synthesized to compare the stabilities and encapsulation properties of the micelles. The synthesis of the EEGE monomer and its subsequent copolymerization with the mPEG macroinitiator (**E** series) were performed following an identical protocol and were confirmed using ^{1}H NMR and GPC techniques (Table 1 and Fig. S4–S6†).

To confirm the presence of the initiator and the successful incorporation of TGE in the PTGE homopolymer, MALDI-TOF spectrometry was performed. As shown in Fig. 3, the molecular weight of 3782.4 g mol^{-1} can be assigned to a polymer chain with 23 repeating units with K^+ as the counterion (benzyl alcohol (108.06 g mol^{-1}) + TGE (158.09 g mol^{-1}) × 23 + K^+ (38.96 g mol^{-1})). Correspondingly, the spacing of the signals is well matched with the molecular weight of the TGE monomer (158.09 g mol^{-1}), which clearly indicates the successful polymerization.

Differential scanning calorimetry (DSC) studies revealed that the glass transition temperatures (T_g) of the PEG-*b*-PTGE block copolymers (**T** series) with a cyclic PTGE block are considerably higher (−16 °C to −21 °C) than those of PEG-*b*-PEEGE (**E** series) with an acyclic PEEGE block (*ca.* −59 °C) (Fig. S8†).[49] In agreement with our observation, Tian *et al.* reported that the T_g values of polyphosphazenes with cyclic pendant groups are higher than those of the linear analogue.[50] We attribute the higher T_g values of the **T** series polymers compared to the **E** series to the cyclic moieties that lead to fewer degrees of conformational freedom, which results in higher energy barriers to torsional motion. Moreover, the possibility of chair-to-chair stacking between side chains could contribute to higher T_g values, while the torsional flexibility of the **E** series with an acyclic analogue led to lower T_g values.[50] In addition, the T_g of the PEG block was not clearly detected in

our system although it was reported around −65 °C in the literature.[51]

2.2 Self-assembly behavior

The critical micelle concentration (CMC) is an important indicator for demonstrating the self-assembly and stability of the micelles.[52] The CMCs of **T** and **E** series of amphiphilic block copolymers were determined *via* an established method using pyrene as a fluorescent probe.[53,54] Above a certain concentration of the polymer solution, pyrene can be encapsulated within the hydrophobic core of the micelle, resulting in a dramatic increase in the excitation band intensity (I_{339}/I_{332}, also expressed as I_3/I_1). The I_3/I_1 ratio was plotted as a function of the concentrations of the respective polymers (Fig. 4; see Fig. S9† for the collected spectra). A clear crossover point was observed for all the PEG-*b*-PTGE block copolymers, suggesting the formation of micelles with respective CMC values of 18.1 (**T1**), 9.79 (**T2**), and 0.89 mg L^{-1} (**T3**). The CMC values of PEG-*b*-PTGE decreased upon increasing the number of the hydrophobic blocks. In contrast, **E1** does not show any sign of micelle formation due to the reduced hydrophobicity of the PEEGE block, whereas other polymers with longer PEEGE blocks displayed a CMC of 96.0 (**E2**) and 10.3 mg mL^{-1} (**E3**). It is worth noting that the CMC values for PEG-*b*-PTGE are approximately 10 times lower than those of the PEG-*b*-PEEGE copolymers. This result indicates that the micelles prepared from PEG-*b*-PTGE polymers which contain a more hydrophobic, cyclic tetrahydropyranyl group are more stable and can sustain their integrity upon dilution after systematic injection compared to their acyclic analogue, PEG-*b*-PEEGE. Moreover, considering the flexible and hydrophilic nature of the polymers with all polyether backbones, the CMC values are significantly lower than those of commercial Pluronic copolymers whose values are in a wide range from 4.0 mg L^{-1} to 1.0×10^4 mg L^{-1}.[55]

After confirming successful micelle formation, we performed cryogenic-transmission electron microscopy (cryo-TEM) to elucidate the morphology of the prepared micelles. Cryo-TEM can directly show the micelle structure in a solution state, relatively free from artifacts. It is observed that the water-dissolved hydrophilic shell does not provide enough contrast against the vitrified solution background (Fig. S11†). As shown in Fig. 5, the cryo-TEM images demonstrate that **T1** and **T2** micelles possess a spherical morphology with a core size of approximately 20.4 ± 2.9 nm and 13.4 ± 1.6 nm, respectively. The core size of the micelles of PEG-*b*-PTGE decreased with increasing length of the hydrophobic PTGE block. We postulate that there is enhanced packing of the side chain within the hydrophobic core of the micelle when the degree of hydrophobic PTGE is increased. Interestingly, the cryo-TEM image of **T2** micelles exhibits a uniform spherical morphology with a regularly packed structure (Fig. 5b). The measured diameter of the micelles was 26.1 nm with a 13.4 nm hydrophobic core and a 6.4 nm hydrophilic corona, which is in good agreement with the hydrodynamic diameter (D_h) of 26.2 ± 4.6 nm measured from dynamic light scattering (DLS) (Fig. S12†). Small-angle X-ray scattering (SAXS) was performed in parallel to further characterize the size and the structure of the micelles (detailed analysis is shown in the ESI†). The fitting results show the core diameter of 16.6 nm and 11.0 nm and the overall micelle diameter of 31.4 nm and 26.4 nm for **T1** and **T2** micelles, respectively (Fig. S13†). In addition, spherical structures of micelles were observed by atomic force microscopy (AFM) (Fig. S14†). The diameter of the **T1**, **T2**, and **E2** micelles measured by AFM was 77.2 ± 9.4 nm, 58.7 ± 9.1 nm and 79.0 ± 14.8 nm, respectively.

All micelles met the requirement for size threshold for effective *in vivo* imaging and delivery to avoid recognition by the reticuloendothelial system to enhance the accumulation in tumors by the enhanced permeability and retention (EPR) effect.[56–58] It is also noteworthy that the **T3** micelles exhibited

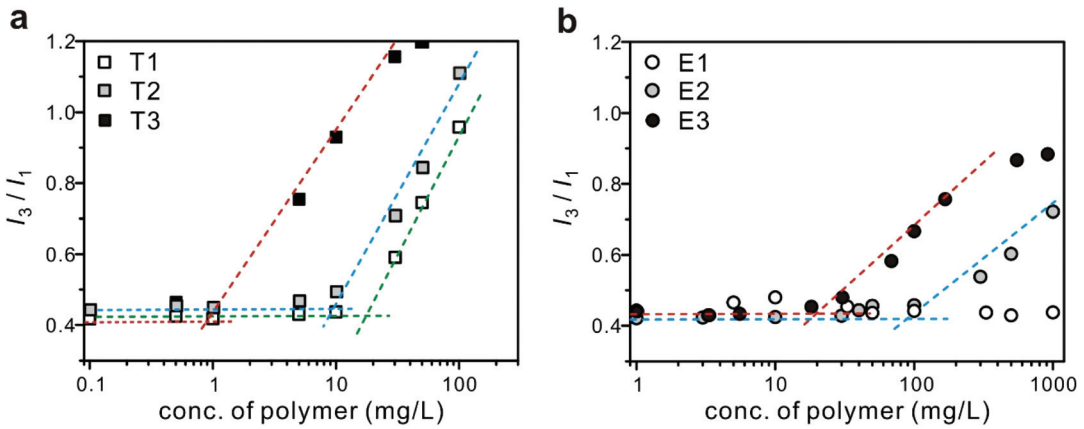

Fig. 4 Determination of CMC for amphiphilic block copolymer micelles *via* measurements of I_3/I_1 as a function of polymer concentration using the fluorescence excitation spectra of pyrene (λ_{em} = 372 nm). (a) **T1** (n = 18), **T2** (n = 37), and **T3** (n = 72) and (b) **E1** (n = 9), **E2** (n = 22), and **E3** (n = 60). n represents the number of respective repeating units in PEG_{114}-*b*-$PTGE_n$ and PEG_{114}-*b*-$PEEGE_n$ (see Table 1 for notation). Dotted lines display the inflection point.

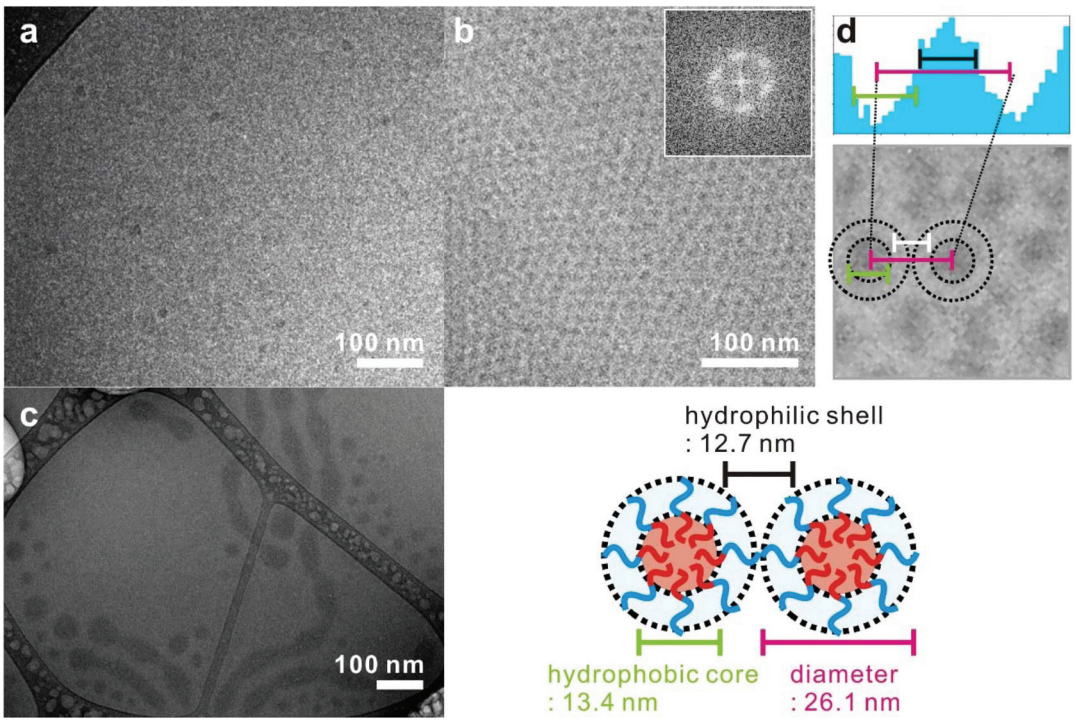

Fig. 5 Representative cryo-TEM images of (a) **T1**, (b) **T2**, (c) **T3** micelles, and (d) schematic representation of the structure of **T2** micelles with dimensions of each block in a micelle. See Fig. S9† for cryo-TEM images of **E2** and **E3** micelles.

mixed morphologies of spherical and cylindrical micelles with increasing size of the hydrophobic block. These results indicate that the polymer composition can control the morphology of PEG-*b*-PTGE micelles, in turn affecting the efficacy of these micelles as drug carriers.[59,60]

2.3 Encapsulation stability of micelles under biological conditions

Among the various factors that determine the suitability of a drug delivery carrier, encapsulation stability under biological conditions is regarded as critical.[61] When considering the diversity of biological encounters that arise during delivery, the encapsulation of hydrophobic components is often challenged by proteins in the blood stream. For example, serum protein adsorption often induces premature release before reaching the target site due to partitioning effects.[62] To investigate the stability of micelles under harsh biological conditions, a Förster resonance energy transfer (FRET)-based method was used in this study as reported previously.[62] The FRET pair comprising the donor, 3,3′-dioctadecyloxacarbocyanine perchlorate (DiO), and the acceptor, 1,1′-dioctadecyl-3,3,3′,3′-tetramethyl indocarbocyanine perchlorate (DiI), was used to assess the loading stability of the prepared micelles. If the micelles are stable, the FRET pair will display a strong emission at 564 nm (emission of the DiI acceptor) resulting from an effective energy transfer due to the proximity of the molecules within the micelle. On the other hand, if the micelles tend to be unstable, the FRET molecules are released, eliminating the FRET effect so that only the emission of the FRET donor, DiO, is observed at 510 nm.

Here, we choose **T1**, **T2**, **T3** and **E3** micelles to compare the stability based on the loading efficiency determined by the model hydrophobic drug, Nile red, within the micelles. Interestingly, the **T1**, **T2**, and **T3** micelles displayed an encapsulation efficiency of 8.2, 14.9, and 16.6% for Nile red, respectively, whereas the **E2** and **E3** micelles showed a relatively lower encapsulation efficiency of 0.50 and 10.9%, respectively (Fig. S15†). It could be attributed to the structural difference and enhanced hydrophobicity of the cyclic PTGE block. Under a similar block length of PEEGE with PTGE, the **E3** micelle showed lower encapsulation efficiency compared to the **T2** micelle, suggesting the important role of the hydrophobic PTGE block in the enhanced loading ability of the hydrophobic encapsulant.

As shown in Fig. 6, the **T1**, **T2**, and **T3** micelles show almost intact FRET emission in phosphate-buffered saline (PBS) as the spectra are dominated by the emission of the FRET acceptor, DiI at 570 nm. As mentioned above, the spectral profile originates from the inter-molecular energy transfer between adjacent DiO and DiI in the micelle core, which suggests excellent stability of the micelles in PBS over 24 h. On the other hand, **E3** micelles exhibited considerable changes in the FRET pattern over time, revealing structural instability in PBS.

When the stability assay was performed in pure serum, the fluorescence intensities of the **T1** and **E3** micelles changed significantly, indicating rapid partitioning of the internal payload among proteins like albumin and globulins present in the

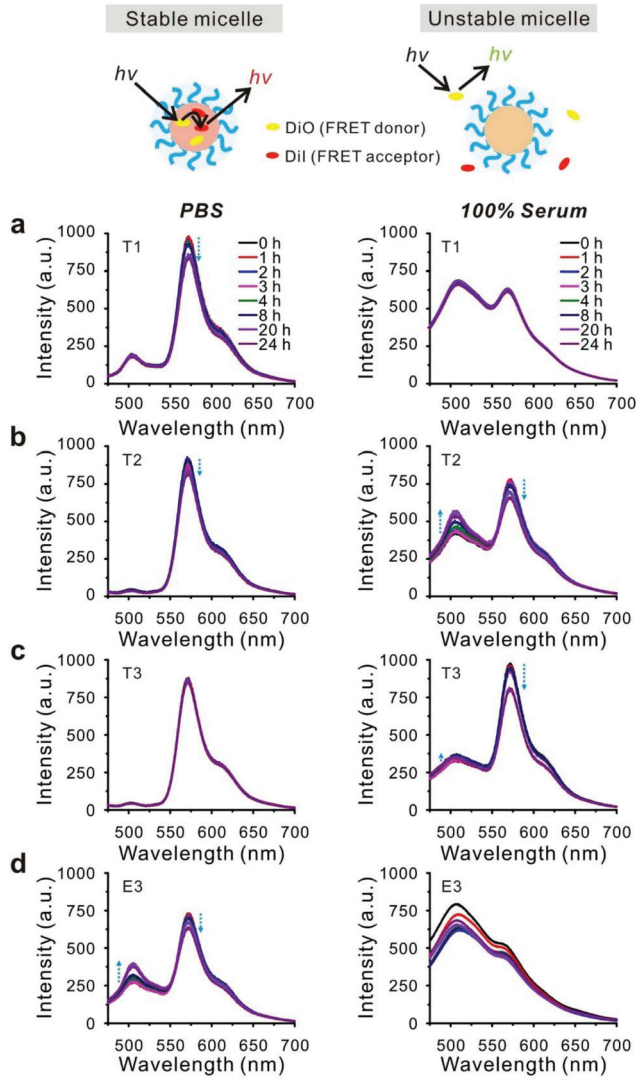

Fig. 6 FRET based encapsulation stability analysis of various micelles under biological conditions using the fluorescence emission spectra (λ_{ex} = 450 nm). (a) **T1**, (b) **T2**, (c) **T3**, and (d) **E3** micelles in (left panel) PBS and (right panel) 100% serum. Emission peak of DiO (FRET donor) observed at 510 nm and DiI (FRET acceptor) at 570 nm.

serum. In clear contrast, the **T3** micelle resisted payload release even for 24 h, highlighting its potential to shield the hydrophobic molecules inside the core from contact with the serum components, thus affording versatile tunability of the release kinetics under biological conditions. A similar phenomenon was observed under 10% and 50% serum conditions (Fig. S16†).

Encouraged by the FRET data on their encapsulation stability, we further examined the stability of the prepared micelles inside cells. The micelles loaded with the FRET pair, DiO and DiI, were incubated in human epithelial carcinoma cells (HeLa cells) with different incubation times and imaged without washing the media. As shown in the left panel of Fig. 7, the red signal from the cell membrane showed a strong red fluorescence from DiI due to effective FRET occurring in **T1**, **T2**, and **T3** micelles, whereas the **E3** micelle indicated a rapid loss of the FRET signal in the cell membrane before internalization. This result once again proved that the micelles with the PTGE block demonstrated superior stability even under *in vitro* conditions with HeLa cells. Upon incubation for 6 h, one could even observe some noticeable differences between the micelles of the **T** series. For example, **T1** rapidly released the internal payload, while **T2** and **T3** displayed a slow release even inside the cytosol, indicating the successful cytoplasmic delivery of the active therapeutics with tunable encapsulation stability, which depends on the choice of the hydrophobic block and length (Fig. 7 and Fig. S17†).

2.4 Degradation in acidic environments

For environment-responsive drug delivery systems, pH-sensitive polymeric micelles have attracted considerable attention due to the wide range of pH changes in many specific compartments.[63–68] In this study, owing to the nature of acetal linkages placed in the side chain of both the PTGE and PEEGE blocks, we pursued the degradation of the amphiphilic block copolymers upon treatment with acid to dissociate the acetal linkages, which resulted in the changes of the hydrophobic PTGE or PEEGE block to its corresponding hydrophilic linear PG block.

Using pyrene as a model hydrophobic therapeutic, the degradation of **T2** micelles was initially monitored in PBS buffer (pH 5.8), which showed a marked stability over 1 week (data not shown). Thus, we employed more acidic conditions (pH 3.0) to highlight the difference between the cyclic PTGE block and the acyclic PEEGE block in terms of their degradation kinetics, although it is beyond the typical biological pH window. After lowering the pH, the intensity of the fluorescence excitation band shifted and decreased with time (Fig. S18†). The change in the excitation band is shown in Fig. 8, in which the ratio of the fluorescence intensity at 339 and 332 nm (I_3/I_1) was plotted as a function of time. Interestingly, the I_3/I_1 plots of **T1** and **T2** micelles with respect to time showed sustained release, which can help maintain therapeutic doses for extended periods within the desirable concentration window for effective drug delivery. It is worth mentioning that the **T3** micelle with the longest hydrophobic block did not release the internal payload even after 7 days under an identical acidic environment (Fig. 8d). These results suggest that the release kinetics can be easily controlled by the number of hydrophobic TGE units. In clear contrast, **E2** micelles showed a burst release only after 5 min of acid treatment, even when the concentration of the polymer was increased to 5 mg mL^{-1} (Fig. 8f). **E3** micelles with a longer hydrophobic block exhibited rapid release of the encapsulated pyrene compared to **E2** micelles, however, the release kinetics was still faster than those of the **T** series micelles (Fig. 8g). It can be postulated that the acid cannot readily penetrate the hydrophobic domain due to the close packing and increased torsional strain of PTGE blocks within the micelle core, thus reducing the access of acid for the hydrolytic degradation of labile acetal linkages. These

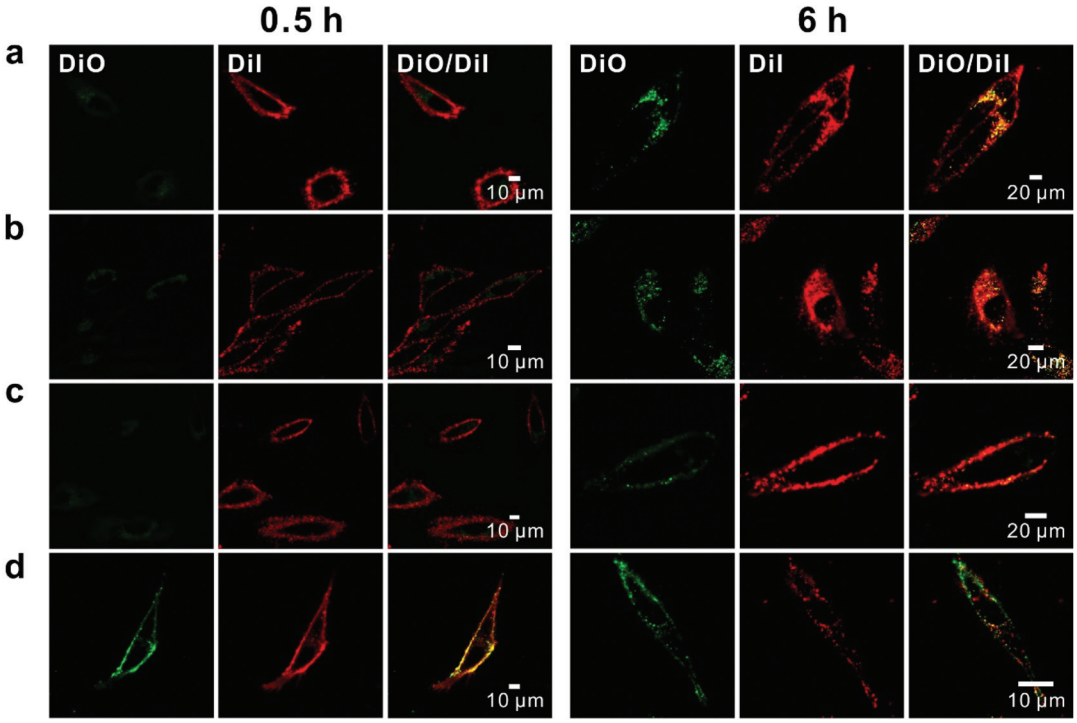

Fig. 7 *In vitro* FRET studies for various micelles. (a) **T1**, (b) **T2**, (c) **T3**, and (d) **E3** micelles after 30 min and 6 h incubation by live imaging in HeLa cells with 10% fetal bovine serum (FBS). Excitation and emission wavelengths for DiO were 488 nm and 535 nm, and those for DiI were set to 543 nm and 620 nm, respectively. See Fig. S16† for images after 12 h incubation.

observations are in line with the results reported by De Geest and co-workers for the hydrolysis of the PTX–polymer conjugates with an acetal linker,[21] and also by Kizhakkedathu and co-workers for the degradation study of the branched polyether with various ketal group structures,[23] and to optimize a wide window of the release kinetics with respect to targeted pH ranges, the synthesis of copolymers with tailorable fraction of cyclic and acyclic analogues is currently underway.

Taken together, we propose that the dramatic difference in the stability and degradation kinetics of different micelles can be attributed to the structural differences between the monomer units of cyclic PTGE and acyclic PEEGE blocks such as hydrophobicity and chain flexibility. The enhanced hydrophobicity of the cyclic PTGE block can be quantitatively calculated based on the partition coefficient, log *P*, using a well-known computational model, ALOGPS 2.1.[69,70] For example, the log *P* value of the cyclic and acyclic monomers was calculated as 0.66 and 0.45, respectively, suggesting enhanced hydrophobicity of the cyclic PTGE block, which in turn contributed to the stability of the micelles and the sustained release kinetics in PEG-*b*-PTGE micelles. Furthermore, the reduced chain flexibility of the cyclic PTGE block was clearly reflected in the higher T_g values together with the stacking between the cyclic PTGE monomer side chains,[54] which may also contribute to the close packing within the micelle core.

2.5 Cell viability test

Finally, we evaluated the cell viability of all the micelles to determine the possibility of using them as drug delivery carriers. Each micelle was treated with HeLa cells to investigate their viability using the well-known MTT assay. As shown in Fig. 9, the cell viability after treating the micelle solution with varying concentrations was nearly 100% in the **T1**, **T2** and **E2** micelles, even at a high concentration of 500 μg mL^{-1}. However, the cell viability of **T3** and **E3** micelles (micelles having a longer hydrophobic chain) decreased slightly for the 250 μg mL^{-1} concentration. This can be explained by the fact that long hydrophobic chains could have a negative effect on biocompatibility; thus, micelle stability and biocompatibility should be optimized to achieve the best performance as drug delivery carriers. Moreover, according to the recent report by Xia *et al.* which demonstrated the cytotoxicity occurring from the residual phosphazene base,[71] the residual phosphazene base was thoroughly removed from the polymers as evidenced by the ^{1}H NMR spectra (Fig. S19†).

Furthermore, we demonstrated the therapeutic effect of micelles loaded with paclitaxel, the poorly water-soluble anticancer drug. We treated the HeLa cell with paclitaxel-loaded micelles to confirm the *in vitro* drug delivery efficiency (Fig. S20†). After 24 h of incubation, the cell viability decreased in all micelles, with the **T** series micelles showing particularly better efficiency compared to the **E** series micelles. This dis-

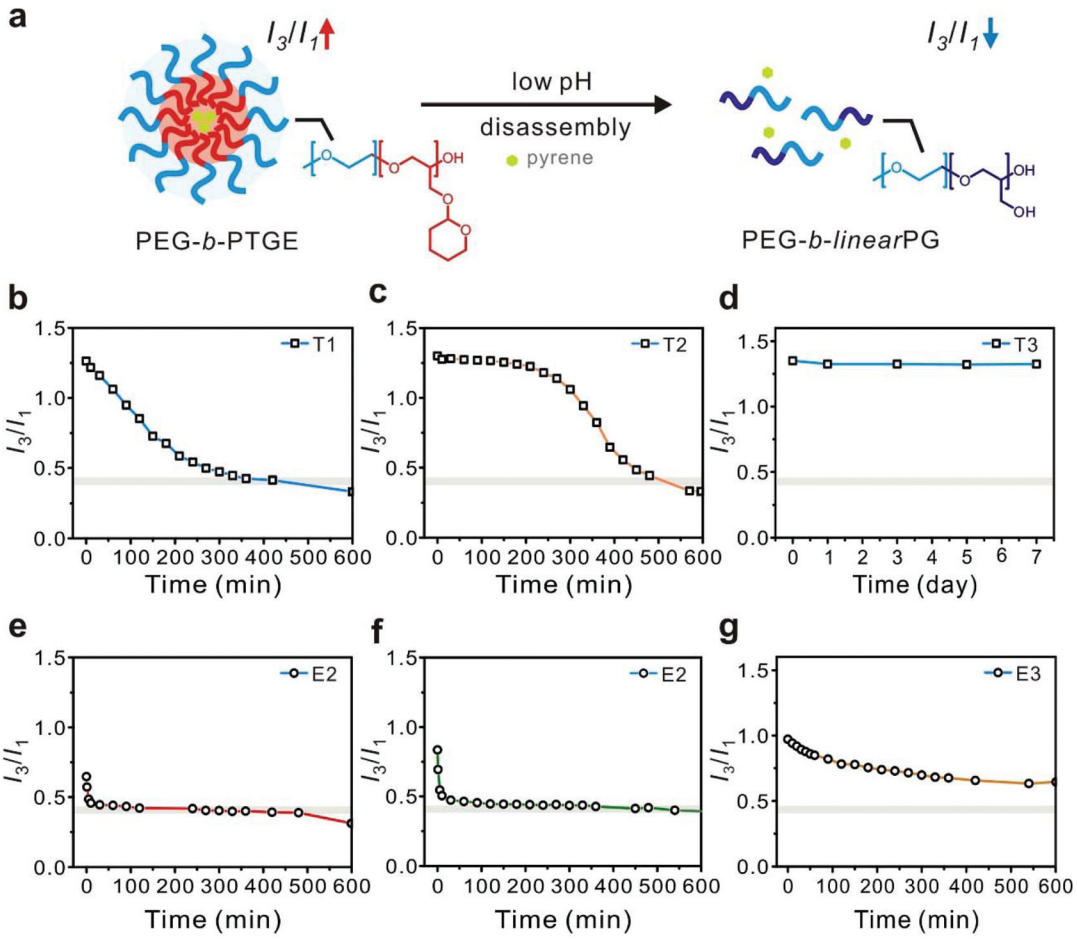

Fig. 8 (a) Illustration of pyrene release upon acid treatment of PEG-*b*-PTGE micelles to form PEG-*b*-linear PG polymers. Plot of I_3/I_1 of pyrene *versus* time under acidic conditions for (b) **T1**, (c) **T2**, (d) **T3**, (e) **E2**, (f) **E2**, and (g) **E3**. All polymers have the concentration of 1.0 mg mL^{-1} except the sample in (f), which has a concentration of 5.0 mg mL^{-1}. The gray line in each graph indicates the I_3/I_1 value of the free pyrene in water. Note that the scale for (d) is expressed in days.

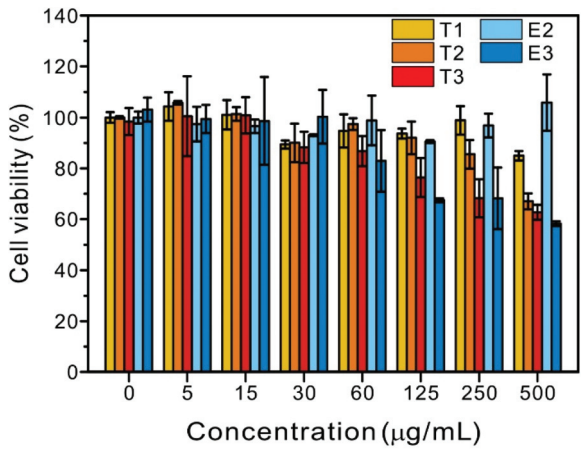

Fig. 9 *In vitro* cell viability assay of all block copolymer micelles determined by the MTT assay using HeLa cells.

tinct difference is due to the higher loading efficiency of the **T** series micelles compared to the **E** series micelles, which confirms their ability to deliver the drug effectively.

3. Conclusions

In summary, we present the synthesis of a novel, versatile epoxide monomer, tetrahydropyranyl glycidyl ether (TGE), in this study. The organic superbase prompted anionic ring-opening polymerization yielded a well-defined PTGE homopolymer and an amphiphilic block copolymer of PEG-*b*-PTGE with controlled molecular weights and low molecular weight distributions. The block copolymer micelles prepared from a series of PEG-*b*-PTGE polymers exhibited superior stability, loading efficiency, and degradation kinetics compared to the micelles prepared from PEG-*b*-PEEGE, containing the acyclic analogue of the PEEGE block. The enhanced stability and tun-

ability of the PTGE block are attributed to its increased hydrophobicity as well as the tight association between the chair conformations of the cyclic TGE side chains. The high stability together with the high biocompatibility clearly demonstrates the significant potential of PEG-*b*-PTGE polymers in drug delivery. We anticipate that a new class of functional epoxide monomers and polymers developed in this study will contribute to the advancement of polyethers and will be promising candidates for emerging materials and biomedical applications.

4. Experimental section

4.1 Materials

All reagents and solvents were purchased from Sigma-Aldrich and Acros and used as received unless otherwise stated. Dry THF and dichloromethane were collected from a solvent drying system and used immediately thereafter. All deuterated NMR solvents such as $CDCl_3$ and D_2O were purchased from Cambridge Isotope Laboratories.

4.2 Characterization

^{1}H-NMR (400 MHz) and ^{13}C-NMR spectra (100 MHz) were acquired using a 400-MR DD2 spectrometer. All spectra were recorded in ppm units with TMS as an internal standard in the deuterated solvents, $CDCl_3$ and D_2O. The number-(M_n) and weight-(M_w) averaged molecular weights and molecular weight distribution (M_w/M_n) were measured using gel permeation chromatography (GPC, Agilent 1200 series). GPC measurements were performed in THF as an eluent at room temperature at a flow rate of 1.0 mL min^{-1} using a refractive index (RI) detector. All calibrations were carried out using polystyrene standards. Differential scanning calorimetry (DSC) was performed under a nitrogen atmosphere using a differential scanning calorimeter (Q200 model, TA Instruments) in the temperature range of −80 °C to 65 °C, at a heating rate of 10 K min^{-1}. Matrix-assisted laser desorption and ionization time-of-flight (MALDI-TOF) mass spectrometry were performed using an Ultraflex III MALDI mass spectrometer with α-cyano-4-hydroxycinnamic acid as the matrix. The excitation spectra of pyrene used in CMC measurements and the emission spectra of Nile red used to calculate encapsulation efficiency were recorded using a fluorometer (RF-6000, Shimadzu). Size distribution analysis of the self-assembled micelles was performed using dynamic light scattering (DLS, BI-APD, Brookhaven Instrument) at angles of 90° and 30°.

4.3 Chemical synthesis

4.3.1 Synthesis of the TGE monomer. A solution of glycidol (10.1 g, 68.0 mmol) and 3,4-dihydro-2*H*-pyran (16.8 g, 200 mmol) in dichloromethane (350 mL) was introduced into a round bottom flask and stirred for 30 min at room temperature. To this solution, *p*-toluenesulfonic acid (0.26 g, 1.38 mmol) was slowly added, followed by overnight vigorous stirring. Then the solution was stirred at room temperature for 1 h after saturated $NaHCO_3$ was added. The aqueous phase was extracted with dichloromethane and the organic layers were extracted with water. The combined organic layers were dried over Na_2SO_4. The organic phase was concentrated under reduced pressure and the residue was purified by flash column chromatography with ethyl acetate/hexane (1 : 8 v/v) as the eluent to obtain 6.45 g (60%) of the TGE monomer as a colorless liquid. Then, the monomer was further purified by distillation. The successful synthesis of the TGE monomer was confirmed by various characterization techniques, including ^{1}H and ^{13}C NMR, COSY, HSQC and ESI-MS (see Fig. 2 for corresponding peak assignments and Fig. S1–S3 in the ESI†). ^{1}H NMR (400 MHz, $CDCl_3$): δ ppm 4.73–4.59 (m, 1H, d), 3.95 (dd, J = 11.7, 3.1 Hz, 0.5H, c), 3.87 (ddd, J = 15.3, 7.8, 3.8 Hz, 1H, e), 3.76–3.66 (m, 1H, c), 3.51 (dt, J = 5.1, 4.4 Hz, 1H, e), 3.40 (dd, J = 11.7, 6.4 Hz, 0.5H, c), 3.19 (tt, J = 7.7, 3.9 Hz, 1H, b), 2.83–2.78 (m, 1H, a), 2.68 (dd, J = 5.2, 2.7 Hz, 1H, a), 2.60 (dd, J = 5.0, 2.7 Hz, 0.5H, a), 1.84 (dd, J = 17.4, 8.6 Hz, 1H, f_3), 1.78–1.67 (m, 1H, f_1), 1.67–1.48 (m, 4H, f_1–f_3). ^{13}C NMR (100 MHz, $CDCl_3$): δ ppm 98.8, 67.9, 62.1, 50.7, 44.5, 30.50, 25.4, 19.3. MS (m/z + Na^+, ESI^+) calcd for $C_8H_{14}O_3$, 181.1; found, 180.6.

4.3.2 Synthesis of the PTGE homopolymer. A 0.25 mL solution of *t*-BuP_4 (0.8 M, 0.20 mmol) in *n*-hexane was added to a 6.94 mL solution of benzyl alcohol (20.7 μL, 0.20 mmol) in toluene under an argon atmosphere. TGE (1.27 g, 8.00 mmol) was then added to the solution dropwise using a syringe pump to initiate the polymerization over 6 h. After stirring at room temperature for 24 h, the polymerization was quenched by the addition of excess benzoic acid. After precipitation in hexane, the mixture was passed through an alumina pad using tetrahydrofuran (THF). The polymer solution was then evaporated to dryness to obtain poly(tetrahydropyranyl glycidyl ether), PTGE (851 mg). Yield: 69.8%. The M_n of PTGE (polymer 3) was 6100 g mol^{-1}, as calculated from the NMR data shown in Fig. 1 using the following equation: number of repeating units (TGE) = 18.9 (integration value) × 2 (number of protons of methylene of benzyl alcohol) = 38; M_n = 158.20 (molecular weight of the TGE monomer) × 38 + 108.14 (molecular weight of benzyl alcohol) = 6119.74 g mol^{-1}. Considering the error range of NMR integration, we used 6100 g mol^{-1} as the M_n value of the PTGE (polymer 3 in Table 1).

4.3.3 Deprotection of PTGE. A solution of PTGE (0.50 g, $M_{n,NMR}$ = 6100 g mol^{-1}) in HCl/MeOH (1.25 M, 0.13 mL) was stirred at room temperature for 2 h. The reaction mixture was neutralized with potassium carbonate. The mixture was filtered and precipitated in excess cold diethyl. The resultant polymer was dried under vacuum for 1 day to obtain linear polyglycerol (210 mg). Yield: 82.3%. The M_n of the resultant polymer was determined to be 3100 g mol^{-1} using NMR data.

4.3.4 Synthesis of the PEG-*b*-PTGE block copolymer. Block copolymer synthesis was conducted using poly(ethylene glycol) methyl ether (mPEG) as a macroinitiator using the same procedure as for the synthesis of the homopolymer. mPEG (0.50 mg, 0.10 mmol) was placed in a flask under argon flow. Toluene (3.47 mL) was then added into the flask and heated

up to 60 °C. After cooling at room temperature, 0.13 mL of *t*-BuP_4 in *n*-hexane (0.8 M, 0.10 mmol) was added to the solution. Then, TGE was added to the solution dropwise using a syringe pump for 6 h. After stirring at room temperature for 24 h, the polymerization was quenched by the addition of benzoic acid. The mixture was precipitated in hexane and passed through a pad of alumina with THF. The polymer solution was evaporated to dryness to obtain poly(ethylene glycol)-*b*-poly(tetrahydropyranyl glycidyl ether), PEG-*b*-PTGE (647 mg). Yield: 74.4%. The M_n of PEG-*b*-PTGE (polymer 5) was determined to be 8700 g mol^{-1}, as calculated from the NMR data (see Fig. 1) using the following equation: number of repeating units (TGE) = 5.89 (integration value) × 3 (number of protons of methyl of mPEG) = 18; M_n = 158.20 (molecular weight of the TGE monomer) × 18 + 5900 (molecular weight of the mPEG macroinitiator) = 8747.6 g mol^{-1}. Considering the error range of NMR integration, we used 8700 g mol^{-1} as the M_n value of the PEG-*b*-PTGE (polymer 5 in Table 1).

4.3.5 Synthesis of the PEG-*b*-PEEGE block copolymer. The PEG-*b*-PEEGE block copolymer was synthesized using the same method as for polymerization of the PEG-*b*-PTGE block copolymer. mPEG (0.50 mg, 0.10 mmol) was placed in a flask under argon flow. Toluene (3.47 mL) was then added into the flask and heated up to 60 °C. After cooling at room temperature, 0.13 mL of *t*-BuP_4 in *n*-hexane (0.8 M, 0.10 mmol) was added to the solution. Then, EEGE was added to the solution dropwise using a syringe pump for 6 h. After stirring at room temperature for 24 h, the polymerization was quenched by the addition of benzoic acid. The mixture was precipitated in hexane and passed through a pad of alumina with THF. The polymer solution was evaporated to dryness to obtain poly (ethylene glycol)-*b*-poly(ethoxyethyl glycidyl ether), PEG-*b*-PEEGE (672 mg). Yield: 73.8%. The M_n of PEG-*b*-PEEGE (polymer 9 in Table 1) was determined to be 9100 g mol^{-1}, as calculated from the NMR data (see Fig. 1) using the following equation: number of repeating units (EEGE) = 7.26 (integration value) × 3 (number of protons of methyl of mPEG) = 22; M_n = 146.19 (molecular weight of the TGE monomer) × 22 + 5900 (molecular weight of the mPEG macroinitiator) = 9116.2 g mol^{-1}. Considering the error range of NMR integration, we used 9100 g mol^{-1} as the M_n value of the PEG-*b*-PEEGE (polymer 9 in Table 1).

4.4 Micelle characterization

4.4.1 Micelle formation and characterization. A 5.0 mg sample of the PEG-*b*-PTGE block copolymer was dissolved in 200 μL of DMF, after which 5 mL of water was added dropwise over 1 h *via* a syringe pump to form micelles. After stirring overnight, the polymer solution was dialyzed against deionized water for 2 days to remove residual DMF. The resultant solution was then filtered through a 0.45 μm syringe filter before DLS, AFM and TEM analysis.

4.4.2 Pyrene fluorescence measurements and CMC studies. A series of polymer solutions in DMF at various concentrations were prepared. A 10 μL solution of pyrene (5.2 mg L^{-1} in DMF) was added to the solution of PEG-*b*-PTGE and the mixture was stirred for 30 min at room temperature. A total of 5.0 mL DI water was then added to the solution at a rate of 0.5 mL min^{-1} using a syringe pump. The solution was left to equilibrate overnight. The fluorescence of each pyrene-containing polymer micelle solution (with different concentrations) was measured at an emission wavelength of 372 nm using a fluorimeter (RF-6000, Shimadzu) through a 1 × 1 cm quartz cell. The following parameters were chosen: emission wavelength = 372 nm, excitation wavelength range = 360–372 nm, scan speed = 600 nm min^{-1}, and data interval = 0.5 nm. The ratio of the fluorescence intensities at wavelengths of 339.5 and 332.5 nm were plotted *versus* the polymer concentrations and the critical micelle concentration was determined from the inflection point.

4.4.3 Conventional TEM measurements. A drop of aqueous solution containing either the PEG-*b*-PTGE block copolymer or the PEG-*b*-PEEGE block copolymer was placed on a formvar/carbon-coated copper grid and allowed to evaporate under ambient conditions. To stain the sample, a drop of uranyl acetate solution (2 wt%) was placed onto the surface of the sample-loaded grid. The staining agent was deposited for at least 3 min, after which the excess solution was wicked off using filter paper. The specimen was observed with a JEM-1400 microscope (JEOL, Tokyo, Japan) operating at 120 kV. The data were analyzed using the Simple Measure program.

4.4.4 Cryo-TEM measurements. Cryo-TEM experiments were performed with a thin film of aqueous solution (3 μL) of the PEG-*b*-PTGE block copolymer or PEG-*b*-PEEGE block copolymer transferred to a lacey carbon supported grid by the plunge-dipping method. The thin aqueous films were prepared at ambient temperatures and with a humidity of 97–99% within a custom-built environmental chamber in order to prevent evaporation of water from the sample solution. The excess liquid was blotted with filter paper for 3 s, and the thin aqueous films were rapidly vitrified by plunging them into liquid ethane (cooled by liquid nitrogen) at its freezing point. The grid was transferred to a Gatan 626 cryo-holder, using a cryo-transfer device. Direct imaging was carried out using a JEM-3011 HR microscope (JEOL, Tokyo, Japan) with a 300 kV accelerating voltage at a temperature of approximately −175 °C. Micrographs were acquired with an SC 1000 CCD camera (Gatan, Inc., PA) and the data were analyzed using the Gatan Digital Micrograph program.

4.4.5 SAXS analysis. SAXS measurement was performed on beamline 4C SAXS at Pohang Acceleration Laboratory (PAL) using 16.9 keV radiation corresponding to a wavelength, λ, of 0.734 Å. The sample-to-detector distance was 4.3 m to cover q range of 0.007 $Å^{-1} < q < 0.12$ $Å^{-1}$, where q is the scattering vector defined as $q = 4\pi\lambda^{-1}\sin(\theta/2)$. The micelle solutions were loaded and sealed into capillary tubes, and followed by exposure to X-ray for 1–2 min. Two-dimensional images were azimuthally averaged to provide a one-dimensional plot of intensity *versus* q. The solvent background, *i.e.*, water, was subtracted from the solution scattering. Based on the cryo-TEM images and DLS data, SAXS profiles obtained from **T1** and **T2**

micelles were simulated by the model including spherical cores with constant shell thickness as shown below:

$$F(q) = \left[\frac{3 \times V_c(\rho_c - \rho_s) j(qR_c)}{qR_c} + \frac{3 \times (V_s(\rho_s - \rho_{sol}) j(qR_s))}{qR_s}\right]^2$$

where

$$j(x) = \frac{\sin x - x \cos x}{x^2},\ V_x = 4/3\pi \times {R_x}^3$$

where V_c, V_s, R_c, and R_s are the volume of the core and shell, and the radius of the core and shell, respectively. Also, ρ_c, ρ_s and ρ_{sol} are the electron density of the core, shell, and solvent, respectively. Schulz distribution of the core radius was employed to take into account the polydisperse core radius.

The solid curves in Fig. S12† represent the best fit to the model. We observed a core diameter of 16.6 nm and 11.0 nm for **T1** and **T2** micelles, respectively, and the overall micelle diameter of 31.4 nm and 26.4 nm for **T1** and **T2** micelles, respectively. These SAXS results show good agreement with the TEM and DLS results.

4.4.6 Encapsulation efficiency. The encapsulation efficiency (EE) of the micelles was calculated from the fluorimeter analysis results as follows. A 0.50 mL solution of Nile red (50 μg mL^{-1} in acetone) was added to a solution of PEG-*b*-PTGE in acetone and the mixture was stirred for 30 min at room temperature. A total of 5 mL deionized water was then added to the solution at a rate of 0.5 mL min^{-1} using a syringe pump. After addition, the solution was left to equilibrate overnight allowing the acetone to evaporate with the lid open. After filtration using a 0.45 μm syringe filter, the solution was lyophilized and redissolved in acetone. The amount of the Nile red loaded in the micelles was determined by fluorometer measurements (RF-6000, Shimadzu) through a 1 × 1 cm quartz cell as follows:

$$\text{EE}\ (\%) = \frac{\text{concentration of drug measured}}{\text{concentration of drug added}} \times 100$$

The following parameters were chosen: excitation wavelength = 480 nm, emission wavelength range = 500–800 nm, scan speed = 2000 nm min^{-1}, and data interval = 0.5 nm.

4.4.7 Encapsulation stability in PBS and serum conditions. A total 1.0 mL solution mixture of DiI and DiO (each 0.50 mL solution of 0.10 mg mL^{-1} in DMF) was added to 0.2 mL solution of PEG-*b*-PTGE (25 mg mL^{-1} in DMF) and the mixture was stirred for 30 min at room temperature. A total of 5 mL deionized water was then added to the solution at a rate of 0.50 mL min^{-1} using a syringe pump. After stirring overnight, the solution was dialyzed against deionized water for 2 days to remove residual DMF. The resultant solution was then filtered through a 0.45 μm syringe filter. A total 200 μL of the micelle solution was mixed with 800 μL of respective buffers of PBS, 10% FBS, 50% FBS or 100% FBS. The stability of different micelles loaded with both DiI and DiO was analyzed for a period of 24 h at room temperature. The excitation was set at 450 nm and the emission was detected from 460 nm to 700 nm using a spectrofluorometer.

4.4.8 *In vitro* imaging of cells incubated with DiO/DiI loaded micelles. HeLa cells (purchased from the Korea Cell Line Bank) were cultured in Dulbecco's modified Eagle's medium (DMEM) supplemented with 10% fetal bovine serum (FBS) and 1% penicillin–streptomycin (Invitrogen Life Technologies, Korea). The cells were maintained under a humid atmosphere containing 5% CO_2 at 37 °C, with the medium changed every other day. The cells were cultured on eight well Lab-Tek glass chamber slides (Thermo Fisher Scientific, Korea). Then the cells were treated with DiI/DiO co-loaded micelles at a concentration of 0.5 μg mL^{-1} and incubated at different time points. The images were captured using the Olympus confocal laser scanning microscope model FV1000 using the excitation filter set to 473 nm.

4.4.9 Pyrene release experiments in acidic environments. A pyrene-containing polymeric micelle solution was prepared according to the procedure described in the CMC study above. To this solution, 0.10 mL of 1 M HCl was slowly added and the changes in excitation spectra were recorded.

4.4.10 *In vitro* cell cytotoxicity. Cytotoxicity tests were carried out to investigate the toxicity of micelles, and their ability as drug delivery carriers using a modified thiazolyl blue tetrazolium bromide (MTT) assay. Briefly, HeLa cells were grown in a 96 well plate with growth medium containing DMEM, 10% FBS, and 1% penicillin–streptomycin at a density of 3×10^4 cells per well. After incubating for 24 h under a humidified atmosphere of 95% air/5% CO_2 for stabilizing the cells, the HeLa cells were treated with each micelle type as well as with paclitaxel-loaded micelles. After 24 h, 10 μL of MTT was added in each well (final conc. of 0.5 mg mL^{-1}), and incubated for 3 h. After that, the culture medium was removed and 100 μL of DMSO was added to each cell well to dissolve the remaining MTT reagent. Finally, the plates were gently agitated for 15 min at room temperature to dissolve the MTT in DMSO. The absorbance was measured at a wavelength of 540 nm using a 620 nm reference.

4.4.11 Preparation of paclitaxel-loaded micelle. A 0.1 mL solution of paclitaxel (1.0 mg mL^{-1} in CH_3CN) was added to a solution of PEG-*b*-PTGE (25 mg) in acetonitrile and the mixture was stirred for 30 min at room temperature. A total 5 mL of deionized water was then added to the solution at a rate of 0.5 mL min^{-1} using a syringe pump. Residual acetonitrile was removed by dialysis for 3 days. After filtration using a 0.45 μm syringe filter, the solution was lyophilized and redissolved in acetonitrile. The encapsulation efficiency (EE) of micelles was calculated by HPLC analysis under the following conditions: acetonitrile/water = 80/20, wavelength = 228 nm.

Conflicts of interest

There are no conflicts to declare.

Author contributions

B.-S. K. conceived of the project, designed experiments, and supervised the project. J. S. synthesized all the compounds,

carried out the experiments, and analyzed the data. L. P. and J.-H. R. conducted the FRET test. Y. C. measured the cell viability. I. K. and E. L. conducted the normal and cryo-TEM. T.-Y. H. and S. C. performed the SAXS measurement. E. A. carried out the AFM measurement. Y. S. helped with the synthesis of the monomer. All the authors discussed the results and commented on the manuscript. The manuscript was written by J. S. and B.-S. K. with input from all the authors.

Acknowledgements

This work was supported by the Samsung Research Foundation (SRFC-MA1602-07).

Notes and references

1 S. Zhang, *Nat. Biotechnol.*, 2003, **21**, 1171–1178.
2 H. Cui, M. J. Webber and S. I. Stupp, *Biopolymers*, 2010, **94**, 1–18.
3 K.-S. Choi, H. C. Lichtenegger, G. D. Stucky and E. W. McFarland, *J. Am. Chem. Soc.*, 2002, **124**, 12402–12403.
4 Y. Lee, T. Ishii, H. J. Kim, N. Nishiyama, Y. Hayakawa, K. Itaka and K. Kataoka, *Angew. Chem., Int. Ed.*, 2010, **49**, 2552–2555.
5 G. Pillai, *SOJ Pharm. Pharm. Sci.*, 2014, **1**, 1–13.
6 J. Liu, F. Zeng and C. Allen, *Eur. J. Pharm. Biopharm.*, 2007, **65**, 309–319.
7 L. Glavas, P. Olsén, K. Odelius and A.-C. Albertsson, *Biomacromolecules*, 2013, **14**, 4150–4156.
8 J. Gou, S. Feng, H. Xu, G. Fang, Y. Chao, Y. Zhang, H. Xu and X. Tang, *Biomacromolecules*, 2015, **16**, 2920–2929.
9 C. Ma, P. Pan, G. Shan, Y. Bao, M. Fujita and M. Maeda, *Langmuir*, 2015, **31**, 1527–1536.
10 X. Zhao, Z. Poon, A. C. Engler, D. K. Bonner and P. T. Hammond, *Biomacromolecules*, 2012, **13**, 1315–1322.
11 N. Dube, J. W. Seo, H. Dong, J. Y. Shu, R. Lund, L. M. Mahakian, K. W. Ferrara and T. Xu, *Biomacromolecules*, 2014, **15**, 2963–2970.
12 Y. Shi, R. van der Meel, B. Theek, E. Oude Blenke, E. H. E. Pieters, M. H. A. M. Fens, J. Ehling, R. M. Schiffelers, G. Storm, C. F. van Nostrum, T. Lammers and W. E. Hennink, *ACS Nano*, 2015, **9**, 3740–3752.
13 Y. Shi, M. J. van Steenbergen, E. A. Teunissen, L. Novo, S. Gradmann, M. Baldus, C. F. van Nostrum and W. E. Hennink, *Biomacromolecules*, 2013, **14**, 1826–1837.
14 M. J. Robb, L. A. Connal, B. F. Lee, N. A. Lynd and C. J. Hawker, *Polym. Chem.*, 2012, **3**, 1618–1628.
15 A. Klaikherd, C. Nagamani and S. Thayumanavan, *J. Am. Chem. Soc.*, 2009, **131**, 4830–4838.
16 E. Fleige, M. A. Quadir and R. Haag, *Adv. Drug Delivery Rev.*, 2012, **64**, 866–884.
17 J. Herzberger, K. Fischer, D. Leibig, M. Bros, R. Thiermann and H. Frey, *J. Am. Chem. Soc.*, 2016, **138**, 9212–9223.
18 S. Son, E. Shin and B.-S. Kim, *Biomacromolecules*, 2014, **15**, 628–634.
19 J. Morsbach, J. Elbert, C. Rüttiger, S. Winzen, H. Frey and M. Gallei, *Macromolecules*, 2016, **49**, 3406–3414.
20 A. Soleimani, A. Borecki and E. R. Gillies, *Polym. Chem.*, 2014, **5**, 7062–7070.
21 B. Louage, M. J. van Steenbergen, L. Nuhn, M. D. P. Risseeuw, I. Karalic, J. Winne, S. Van Calenbergh, W. E. Hennink and B. G. De Geest, *ACS Macro Lett.*, 2017, **6**, 272–276.
22 B. Louage, Q. Zhang, N. Vanparijs, L. Voorhaar, S. Vande Casteele, Y. Shi, W. E. Hennink, J. Van Bocxlaer, R. Hoogenboom and B. G. De Geest, *Biomacromolecules*, 2015, **16**, 336–350.
23 R. A. Shenoi, J. K. Narayanannair, J. L. Hamilton, B. F. L. Lai, S. Horte, R. K. Kainthan, J. P. Varghese, K. G. Rajeev, M. Manoharan and J. N. Kizhakkedathu, *J. Am. Chem. Soc.*, 2012, **134**, 14945–14957.
24 R. A. Shenoi, S. Abbina and J. N. Kizhakkedathu, *Biomacromolecules*, 2016, **17**, 3683–3693.
25 A. J. Harnoy, M. Buzhor, E. Tirosh, R. Shaharabani, R. Beck and R. J. Amir, *Biomacromolecules*, 2017, **18**, 1218–1228.
26 L. Vukovi, F. A. Khatib, S. P. Drake, A. Madriaga and K. S. Brandenburg, *J. Am. Chem. Soc.*, 2011, **133**, 13481–13488.
27 P. Dey, M. Adamovski, S. Friebe, A. Badalyan, R. C. Mutihac, F. Paulus, S. Leimkühler, U. Wollenberger and R. Haag, *ACS Appl. Mater. Interfaces*, 2014, **6**, 8937–8941.
28 A. Thomas, S. S. Müller and H. Frey, *Biomacromolecules*, 2014, **15**, 1935–1954.
29 R. K. Kainthan, J. Janzen, E. Levin, D. V. Devine and D. E. Brooks, *Biomacromolecules*, 2006, **7**, 703–709.
30 C. G. Rodriguez, R. C. Ferrier, A. Helenic and N. A. Lynd, *Macromolecules*, 2017, **50**, 3121–3130.
31 E. M. Christ, D. Hobernik, M. Bros, M. Wagner and H. Frey, *Biomacromolecules*, 2015, **16**, 3297–3307.
32 F. Wurm, J. Nieberle and H. Frey, *Macromolecules*, 2008, **41**, 1184–1188.
33 C. Schüll, T. Gieshoff and H. Frey, *Polym. Chem.*, 2013, **4**, 4730–4736.
34 C. Siegers, M. Biesalski and R. Haag, *Chem. – Eur. J.*, 2004, **10**, 2831–2838.
35 K. Niederer, C. Schu, D. Leibig, T. Johann and H. Frey, *Macromolecules*, 2016, **49**, 1655–1665.
36 T. Isono, S. Asai, Y. Satoh, T. Takaoka, K. Tajima, T. Kakuchi and T. Satoh, *Macromolecules*, 2015, **48**, 3217–3229.
37 S. Song, J. Lee, S. Kweon, J. Song, K. Kim and B.-S. Kim, *Biomacromolecules*, 2016, **17**, 3632–3639.
38 J. Herzberger, K. Niederer, H. Pohlit, J. Seiwert, M. Worm, F. R. Wurm and H. Frey, *Chem. Rev.*, 2016, **116**, 2170–2243.
39 S. Son, E. Shin and B.-S. Kim, *Macromolecules*, 2015, **48**, 600–609.
40 J. Zhang and G. Wang, *Sci. China: Chem.*, 2015, **58**, 1674–1694.

41 D. Taton, A. Le Borgne, M. Sepulchre and N. Spassky, *Macromol. Chem. Phys.*, 1994, **195**, 139–148.
42 B. Liu and S. Thayumanavan, *J. Am. Chem. Soc.*, 2017, **137**, 2306–2317.
43 A. Dworak, B. Trzebicka, W. Walach, A. Utrata and C. Tsvetanov, *Macromol. Symp.*, 2004, **210**, 419–426.
44 Y. Oikawa, S. Lee, D. H. Kim, D. H. Kang, B.-S. Kim, K. Saito, S. Sasaki, Y. Oishi and Y. Shibasaki, *Biomacromolecules*, 2013, **14**, 2171–2178.
45 X. Song, M. Cao, P. Chen, R. Xia, Z. Zheng, J. Miao, B. Yang, L. Su, J. Qian and X. Feng, *Polym. Bull.*, 2017, **74**, 183–194.
46 H. Misaka, E. Tamura, K. Makiguchi, K. Kamoshida, R. Sakai, T. Satoh and T. Kakuchi, *J. Polym. Sci., Part A: Polym. Chem.*, 2012, **50**, 1941–1952.
47 Y. Satoh, K. Miyachi, H. Matsuno, T. Isono, K. Tajima, T. Kakuchi and T. Satoh, *Macromolecules*, 2016, **49**, 499–509.
48 P. Olsén, T. Borke, K. Odelius and A.-C. Albertsson, *Biomacromolecules*, 2013, **14**, 2883–2890.
49 M. Siebert, H. Keul and M. Möller, *Des. Monomers Polym.*, 2010, **13**, 547–563.
50 Z. Tian, A. Hess, C. R. Fellin, H. Nulwala and H. R. Allcock, *Macromolecules*, 2015, **48**, 4301–4311.
51 Y. Xu, Y. He, J. Wei, Z. Fan and S. Li, *Macromol. Chem. Phys.*, 2008, **209**, 1836–1844.
52 S. C. Owen, D. P. Y. Chan and M. S. Shoichet, *Nano Today*, 2012, **7**, 53–65.
53 M. Wilhelm, C.-L. Zhao, Y. Wang, R. Xu, M. A. Winnik, J.-L. Mura;, G. Riess and M. D. Croucher, *Macromolecules*, 1991, **24**, 1033–1040.
54 F. K. Wolf, A. M. Hofmann and H. Frey, *Macromolecules*, 2010, **43**, 3314–3324.
55 A. V. Kabanov, E. V. Batrakova and V. Y. Alakhov, *J. Controlled Release*, 2002, **82**, 189–212.
56 S. Stolnik, L. Illum and S. S. Davis, *Adv. Drug Delivery Rev.*, 2012, **64**, 290–301.
57 R. M. Schiffelers, I. A. Bakker-Woudenberg and G. Storm, *Biochim. Biophys. Acta, Biomembr.*, 2000, **1468**, 253–261.
58 G. Kwon, S. Suwaat, M. Yokoyama, T. Okano, Y. Sakurap and K. Kataoka, *J. Controlled Release*, 1994, **29**, 17–23.
59 K. Zhang, H. Fang, Z. Chen, J. A. Taylor and K. L. Wooley, *Bioconjugate Chem.*, 2008, **19**, 1880–1887.
60 Y. Geng, P. Dalhaimer, S. Cai, R. Tsai, M. Tewari, T. Minko and D. E. Discher, *Nat. Nanotechnol.*, 2007, **2**, 249–255.
61 L. Li and S. Thayumanavan, *Langmuir*, 2014, **30**, 12384–12390.
62 J. Lu, S. C. Owen and M. S. Shoichet, *Macromolecules*, 2011, **44**, 6002–6008.
63 P. Lundberg, N. A. Lynd, Y. Zhang, X. Zeng, D. V. Krogstad, T. Paffen, M. Malkoch, A. M. Nyström and C. J. Hawker, *Soft Matter*, 2013, **9**, 82–89.
64 E. S. Lee, K. Na and Y. M. Bae, *Nano Lett.*, 2005, **5**, 325–329.
65 X. Zhang, Y. Huang, M. Ghazwani, P. Zhang, J. Li, S. H. Thorne and S. Li, *ACS Macro Lett.*, 2015, **4**, 620–623.
66 P. Zhou, Y. Liu, L. Niu and J. Zhu, *Polym. Chem.*, 2015, **392**, 2934–2944.
67 Q. Qi, Y. Li, X. Yan, F. Zhang, S. Jiang, J. Su, B. Xu, X. Fu, L. Sun and W. Tian, *Polym. Chem.*, 2016, **7**, 5273–5280.
68 J. Ma, K. Kang, Q. Yi and Z. Gu, *RSC Adv.*, 2016, **6**, 64778–64790.
69 I. V. Tetko, J. Gasteiger, R. Todeschini, A. Mauri, D. Livingstone, P. Ertl, V. A. Palyulin, E. V. Radchenko, N. S. Zefirov, A. S. Makarenko, V. Y. Tanchuk and V. V. Prokopenko, *J. Comput.–Aided. Mol. Des.*, 2005, **19**, 453–463.
70 *VCCLAB*, Virtual Computational Chemistry Laboratory, http://www.vcclab.org, 2005.
71 Y. Xia, J. Shen, H. Alamri, N. Hadjichristidis, J. Zhao, Y. Wang and G. Zhang, *Biomacromolecules*, 2017, **18**, 3233–3237.

